ESA Contract Report

ESA contract 4000127267/19/NL/AF

Contract Report to the European Space Agency

GRDS test-bed report

Authors: Pete Weston, Patricia de Rosnay and Stephen English
Contract officer: Antonio Martellucci

May 2021

Abbreviations

BUFR	Binary Universal Form for the Representation of meteorological data
CMEM	Community Microwave Emissivity Modelling platform
ECFS	ECMWF's File Storage system
ECMWF	European Centre for Medium-range Weather Forecasts
ESA	European Space Agency
GRDS	Ground RFI Detection System
IFS	Integrated Forecast System
MIRAS	Microwave Imaging Radiometer using Aperture Synthesis
NRT	Near Real Time
NWP	Numerical Weather Prediction
RDA	Research and Development Aerospace
RFI	Radio Frequency Interference
SAPP	Scalable Acquisition and Pre-Processing system
SMOS	Soil Moisture and Ocean Salinity
ZBT	Zenithal Blue Technologies

1. Introduction

This document summarises the results acquired from testing the updated radio frequency interference (RFI) screening from the ground RFI detection system (GRDS) developed by Zenithal Blue Technologies (ZBT) and Research and Development in Aerospace (RDA). Data from the European Space Agency (ESA) Soil Moisture and Ocean Salinity (SMOS) mission is used to assess the RFI screening. At the European Centre for Medium-range Weather Forecasts (ECMWF) SMOS data is routinely monitored by comparing it to high-quality short-range numerical weather prediction (NWP) forecasts. Experiments using this monitoring system have been run to compare the current data quality with the quality of the GRDS screened data.

2. SMOS monitoring at ECMWF

2.1. Operational monitoring of the NRT SMOS brightness temperatures

The GRDS test-bed is based on the operational ECMWF SMOS monitoring system (Muñoz-Sabater et al, 2013) which is part of the ECMWF integrated forecasting system (IFS). The monitoring system runs twice per day at 00UTC and 12UTC and compares SMOS observations with a high-quality stable reference state provided by the short-range operational forecast fields from the IFS. The resolution of the model fields used is $T_{CO}1279$ which is roughly equivalent to each model grid box being 9km x 9km in size. By comparison the SMOS field of view is approximately 50km in diameter. The observation locations are interpolated to model grid point locations and the Community Microwave Emissivity Modelling platform (CMEM) is used as the observation operator to convert model fields of temperature, humidity etc. into equivalent brightness temperatures. This then allows the modelled brightness temperatures to be subtracted from the collocated observed values to calculate what are known as "first-guess departures". Analysing the statistical distributions of these first-guess departures is a key part of assessing the quality of the SMOS observational data. The samples for the statistical analysis can then be split up temporally and geographically as well as by instrument characteristics such as polarisation, incidence angle etc. The various monitoring plots are published online and can be seen at https://www.ecmwf.int/en/forecasts/quality-our-forecasts/monitoring/smos-monitoring. Because the short-range operational forecast, which the SMOS data are compared against, is so stable, any changes in the first-guess departure statistics will indicate changes to the quality of the SMOS data which could represent instrument anomalies, changes in calibration, changes to the screening or improvements in the processing algorithms. In the context of this project the aim is to assess the change in first-guess departure statistics due to the changes to the radio frequency interference (RFI) flags associated with the data.

Currently bits 1, 4 and 9 of the SMOS information flags in the SMOS input BUFR files provide information on whether a SMOS observation is affected by RFI or not. As part of the SMOS pre-processing and pre-screening at ECMWF any SMOS observation which is affected by RFI as indicated by these flags is not processed further and first-guess departure statistics are not calculated for these observations.

In a monitoring context this is done to avoid effects of RFI skewing the first-guess departure statistics. To identify problems with the SMOS data a stable time series of first-guess departures is required. RFI

can vary in time and space and if not properly screened could lead to changes to the first-guess departures which could be mis-interpreted as a problem with the Microwave Imaging Radiometer using Aperture Synthesis (MIRAS) instrument onboard the SMOS satellite. SMOS brightness temperatures are not directly assimilated into any ECMWF model but if they were and RFI-affected observations were assimilated then this could lead to anomalous analysis increments applied to the initial model state and consequent degraded forecasts. These are two reasons why it is important to screen out RFI-affected observations.

The current monitoring plots, e.g. figure 1, show large areas of consistently increased standard deviation of first-guess departures over parts of East Africa, the Middle East and East Asia. It is thought that RFI which is not detected by the existing RFI flags is causing these effects on the data which suggests that the current RFI screening is sub-optimal. Hence the need for updated RFI screening algorithms as provided by the GRDS.
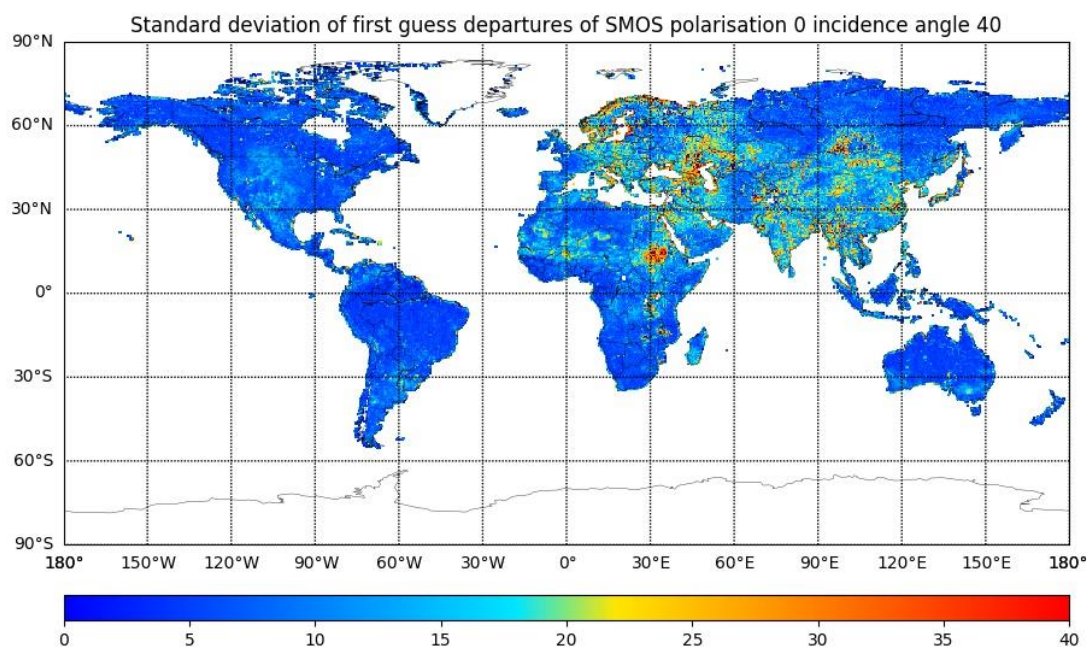

Figure 1: Operational SMOS brightness temperature monitoring: standard deviation of SMOS first-guess departures (K) at H polarisation and incidence angles of 40°±0.5° from 22nd August 2019 to 21st September 2019

2.2.   Experiment setup for the GRDS test-bed

Full details of the test-bed plan can be found in Weston et al. (2020).

The ECMWF Forecast Department have run their acquisition and pre-processing system, SAPP, to process the GRDS generated SMOS BUFR files into a format which can be read into the IFS and the pre-processed BUFR files have been stored on ECMWF's File Storage system (ECFS). The control experiment (CTRL) uses the NRT SMOS level 1 brightness temperature product produced using v6.20 of the SMOS processor. This is the product that has been operationally monitored at ECMWF from

May 2015 to present. The existing RFI screening is relaxed in CTRL whilst retaining the information on which observations have been flagged for RFI. The test experiment (TEST) will use the same NRT SMOS level 1 brightness temperature product with the RFI flags adjusted so that they use the outputs from the GRDS. We currently only use bits 1, 4, 5 and 9 in the SMOS BUFR flag table (de Rosnay et al, 2015) so the other 9 bits have been used to store the GRDS RFI flags with each bit representing a different algorithm. Table 1 shows which GRDS algorithms correspond to which bit numbers.

Bit number	Algorithm
2	Intensity HH / VV (HH/VV brightness temperature exceeding the threshold level N)
3	Intensity T3 (T3 brightness temperature exceeding the threshold level N)
6	Cross polarisation difference exceeding the threshold level N
7	Spatial variability exceeding the threshold level N
8	High pass filter exceeding the threshold level N
10	Intensity T4 (T4 brightness temperature exceeding the threshold level N)
11	STD T4 (Standard deviation of T4 exceeding the threshold level N)
12	Kurtosis T4 (Kurtosis of T4 exceeding the threshold level N)
13	Skewness T4 (Skewness of T4 exceeding the threshold level N)

Table 1: Details of the GRDS algorithms corresponding to the different SMOS information flag bits. Full details of the algorithms can be found in Oliva (2020)

As in CTRL, all RFI screening has been switched off whilst retaining the new RFI flagging information to allow analysis of the full sample of both RFI-affected and non RFI-affected observations. In this way the various RFI bits representing different GRDS algorithms have been assessed separately to ascertain which ones are more important than others. This has helped to consolidate and fine tune the algorithm thresholds in the GRDS, and can be used to devise an optimal strategy for using the 2 bits available for RFI flagging for operational products. Three separate datasets have been provided where different thresholds have been used in the GRDS, these are summarised in table 2.

Both CTRL and TEST experiments run the ECMWF IFS cycle 46r1, the operational configuration between June 2019 and July 2020, at a horizontal resolution of T_L511 (~40km grid spacing), which matches better the SMOS FOV size than the operational resolution ($T_{CO}1279$, ~9km grid spacing). The experiments have been run over a period of one month between 1st July 2019 and 31st July 2019 in order to gain statistically significant results in the comparisons. See appendix A of Weston et al. (2020) for a justification on the use of a one month experimental period. In addition, a number of smaller samples have been provided and tested allowing for significant refinements to the GRDS algorithms and

thresholds prior to the final sample being provided. A brief summary of results from these intermediate versions is provided in appendix A.

Threshold	Description of screening
3	Most conservative threshold, screening the fewest, worst-affected, observations
2	Intermediate threshold, screening more observations than threshold 3
1	Aggressive threshold, screening the most observations

Table 2: Description of the different thresholds used in the GRDS-generated datasets

3. GRDS test-bed results

This section presents analysis of the effect on the first-guess departure statistics of screening SMOS observations based on the new GRDS-based RFI screening flags. The results with the GRDS-based screening are compared to a baseline with no RFI screening and the control with the currently operational RFI screening.

3.1. Global first-guess departure statistics

The following analysis examines the global first-guess departure statistics of data samples screened by the GRDS, compared against the no screening baseline and current screening control. In table 3 and figure 2 the flagging information from the new GRDS algorithms have been combined by considering that if any of the algorithms indicates RFI is present then that observation is screened out. The first-guess departure statistics presented are for the sample of observations considered to be free of RFI i.e those observations where RFI has been detected have been removed from the sample on which the statistics are calculated.

Table 3 shows that for every combination of polarisation and incidence angle, the GRDS screening with the most conservative threshold 3 screens fewer observations than the current screening whilst reducing the standard deviation of first-guess departures by a larger amount. This suggests that, even with the most conservative threshold, the GRDS is outperforming the current screening by removing the observations which are worst affected by RFI and avoiding too many false alarms. For the more aggressive thresholds 2 and 1, more observations are screened, and the standard deviation of first-guess departures are reduced further. This indicates that the GRDS screening is performing as expected and applying more aggressive thresholds leads to more RFI-affected observations being screened out. The effect of the screening on the mean first-guess departures is less clear but the magnitudes of the biases do appear to be reduced for some polarisation and incidence angle combinations especially for V polarisations at 30 and 40 degrees incidence angle. The average fraction of observations screened out by the current flags is 10.3% compared to 7.3%, 12.4% and 24.2% for the GRDS flags with thresholds 1, 2 and 3 respectively.

Polarisation	Incidence angle	RFI flags used	Count	Mean first-guess departure	Standard deviation first-guess departure
H	30	No RFI flag	2163220	-0.04037	19.37803
H	30	Current flags	1979865	0.098623	17.4339
H	30	GRDS flags 3	2010433	-0.07721	16.71456
H	30	GRDS flags 2	1877833	0.079323	16.05344
H	30	GRDS flags 1	1560432	0.388104	15.18065
H	40	No RFI flag	2996653	0.047743	20.13386
H	40	Current flags	2727869	0.131927	18.10779
H	40	GRDS flags 3	2780278	-0.05195	17.39155
H	40	GRDS flags 2	2613579	0.038261	16.78619
H	40	GRDS flags 1	2245698	0.152238	16.1093
H	50	No RFI flag	2013025	-3.13979	21.97319
H	50	Current flags	1828549	-3.03552	19.93742
H	50	GRDS flags 3	1893564	-3.21324	19.54846
H	50	GRDS flags 3	1821996	-3.1694	19.14028
H	50	GRDS flags 3	1650247	-2.90284	18.59731
V	30	No RFI flag	2163232	-2.2375	19.89925
V	30	Current flags	1925358	-1.72393	16.57848
V	30	GRDS flags 3	1995688	-1.80611	15.76196
V	30	GRDS flags 2	1872520	-1.56184	15.02604
V	30	GRDS flags 1	1585329	-1.00552	14.022
V	40	No RFI flag	2993076	-1.17025	19.42083
V	40	Current flags	2642523	-0.7639	15.93211
V	40	GRDS flags 3	2757093	-0.95897	15.18058
V	40	GRDS flags 2	2609980	-0.87514	14.54302
V	40	GRDS flags 1	2271902	-0.672	13.74979
V	50	No RFI flag	2004013	-3.51902	17.9984
V	50	Current flags	1748434	-3.13254	14.05331
V	50	GRDS flags 3	1851273	-3.39627	13.59179
V	50	GRDS flags 2	1761949	-3.45731	13.11454
V	50	GRDS flags 1	1555437	-3.535	12.62966

Table 3: Global SMOS first-guess departure statistics for different combinations of polarisation, incidence angle and RFI screening. The GRDS flags are applied using three different thresholds. Threshold 3 screens the fewest observation, threshold 2 an intermediate number and threshold 1 screens the most observations. The sample of data used in the statistics is from 1st July 2019 to 31st July 2019

Figure 2 illustrates that the GRDS screening with the most conservative threshold is screening out fewer observations whilst reducing the standard deviation of first-guess departures more than the currently operational RFI flags. Again, the more aggressive thresholds 2 and 1 screen more data but further reduce the standard deviation of first-guess departures by a significant amount compared to using no RFI flags or the current flags. This indicates that the GRDS screening is correctly flagging observations in disagreement with the model with the different thresholds performing as expected.
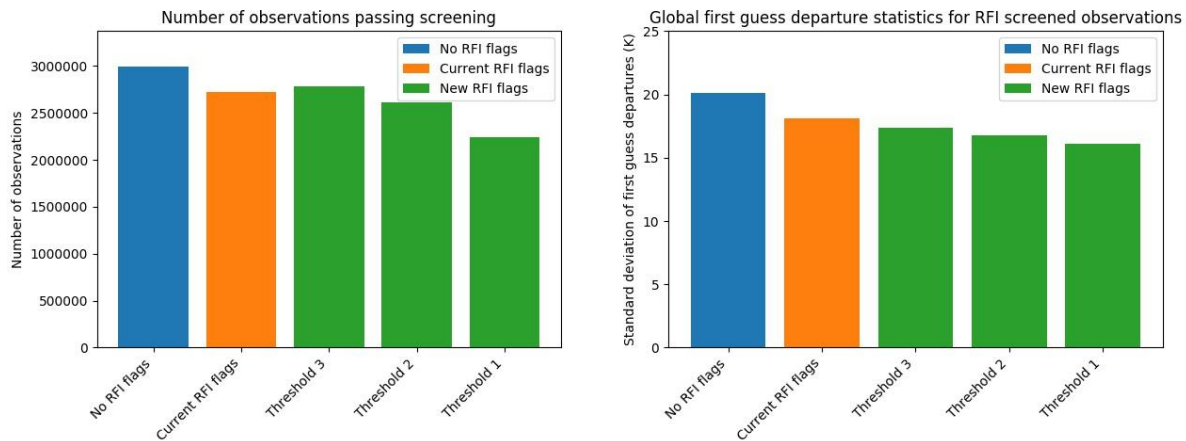
Figure 2: Bar charts showing the number of SMOS observations at H polarisation and incidence angles of 40°±0.5° passing RFI screening (left panel) and the global standard deviation of first-guess departures (right panel) for different versions of RFI screening: No screening (blue bar); current screening (orange bar); GRDS screening with different thresholds (green bars). The data is accumulated from 1st July 2019 to 31st July 2019

Figure 3 shows a breakdown of the performance of each of the different GRDS algorithms detailed in table 1. It shows that RFI flags 7 and 8 are responsible for screening out the most observations. These flags represent the spatial variability and high pass filter algorithms. The next most effective algorithms are RFI flags 2 and 6 representing the intensity HH/VV and cross polarisation algorithms. The remaining algorithms don't screen many observations.

Figure 4 shows the effect the screening from each algorithm has on the standard deviation of first-guess departures. As with the number of observations screened it is clear that flags 2, 6, 7 and 8 all result in a significant reduction in the standard deviation of first-guess departures indicating observations in disagreement with the model are being screened out successfully. However, figure 4 shows that RFI flags 3, 10 and 11 are also having a significant effect on the first-guess departure statistics even though they are not responsible for screening out many observations. These flags represent the intensity T3, intensity T4 and standard deviation algorithms. Figure 4 also shows that RFI flags 12 and 13 representing the kurtosis and skewness algorithms are not having a significant effect on the data quality.

A method for measuring the effectiveness of the individual algorithms is to divide the reduction in standard deviation of first-guess departures by the number of observations screened out. The higher the value of this effectiveness metric the better as this indicates a large effect on the statistics from a smaller number of observations screened. An indicator of false alarms would be a low value of this metric indicating a small effect on the statistics from a large number of observations screened. Figure 5 shows, for all algorithms, that threshold 3 is the most effective followed by thresholds 2 and finally 1. This is to be expected as threshold 3 is expected to remove the observations which are worst affected by RFI with the more aggressive thresholds only additionally screening out observations more subtly affected by RFI. By this metric the most effective algorithms are RFI flags 3 and 10 but all of the flags except for 12 and 13 are performing fairly similarly. This is a good sign that the GRDS is balanced and no single algorithm is dominating the screening. This metric was very useful for improving previous versions of the GRDS as shown in appendix A.
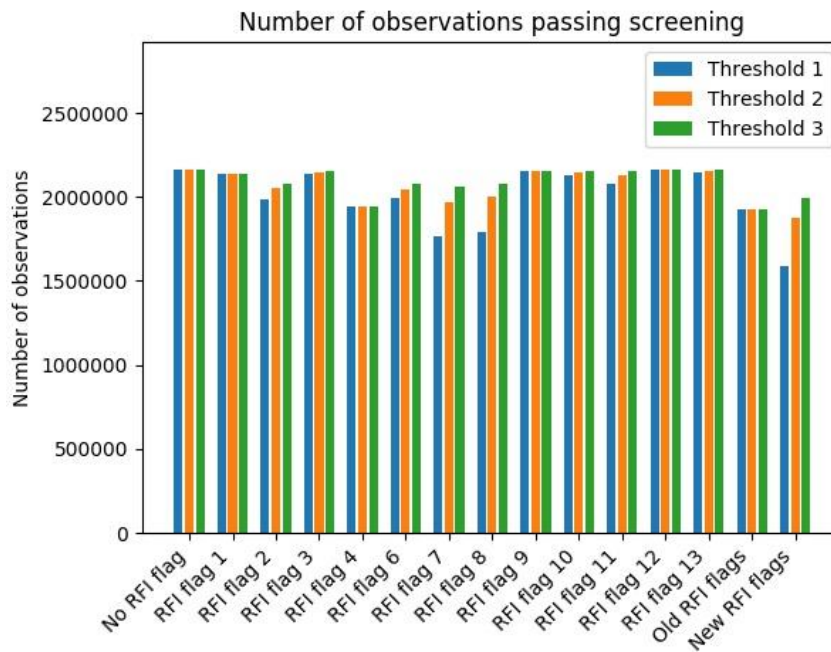
Figure 3: Bar chart showing the number of SMOS observations at V polarisation and incidence angles of 30°±0.5° passing RFI screening for different GRDS algorithms and thresholds. The 2 sets of bars farthest to the right represent the combination of all of the current (old) flags 1, 4 and 9; and the combination of all of the GRDS (new) flags. The data is accumulated from 1st July 2019 to 31st July 2019
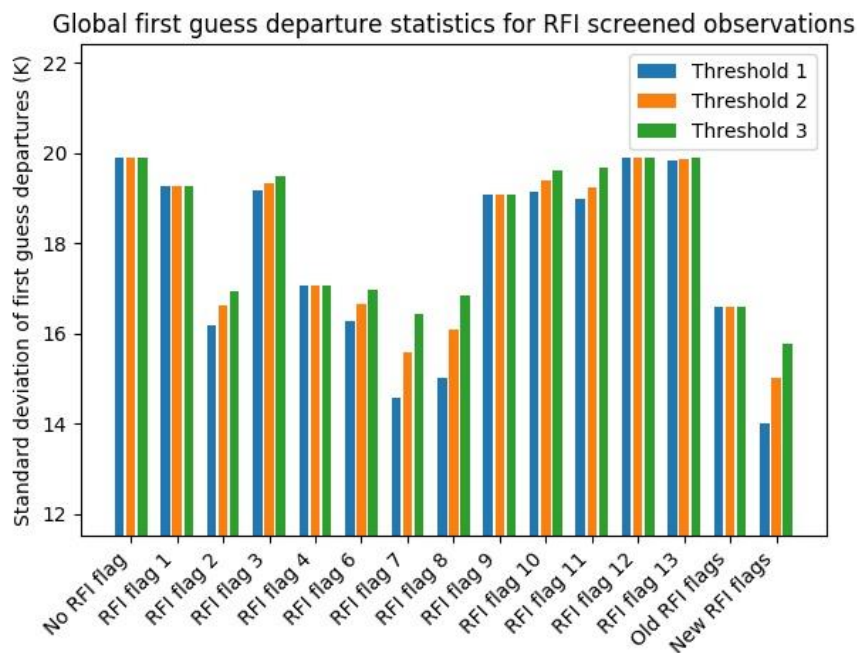

Figure 4: As figure 3 but for the standard deviation of first-guess departures. The data is accumulated from 1st July 2019 to 31st July 2019. Note the shortened y axis scale to highlight the differences between the different algorithms
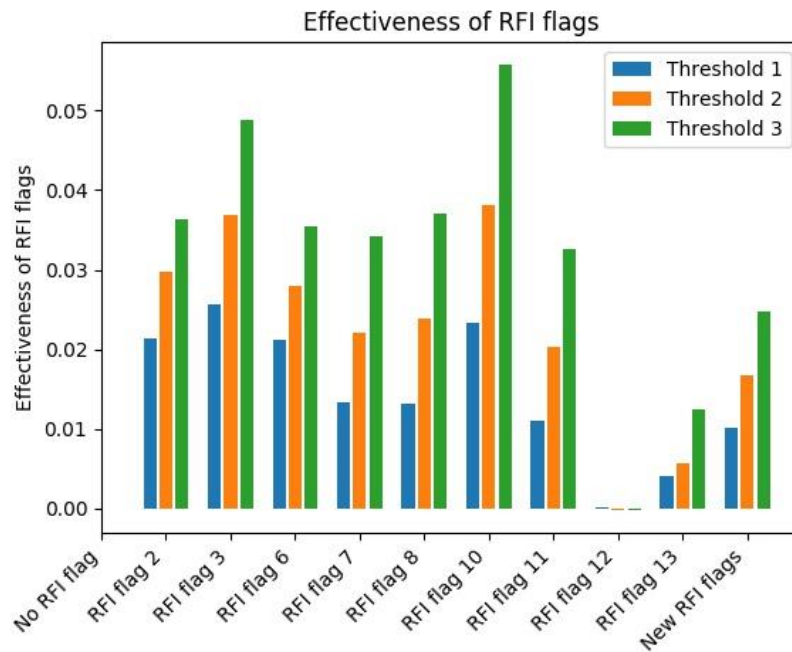
Figure 5: As figure 3 but for the effectiveness metric which is defined as the reduction in standard deviation of first-guess departures divided by the number of observations screened for each algorithm (see main text for full description). The data is accumulated from 1st July 2019 to 31st July 2019
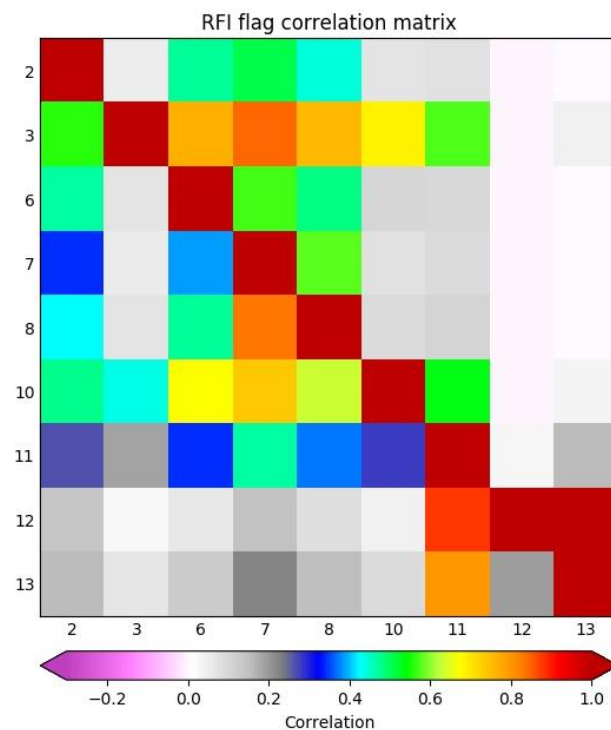

Figure 6: Fraction of observations screened by both algorithms divided by number of observations screened by a single algorithm for each pair of algorithms (rows and columns). The data is accumulated from 1st July 2019 to 31st July 2019

In terms of global statistics one final aspect to examine is how many observations are screened by multiple algorithms and how much unique screening information is each algorithm providing. This can be done for each pair of algorithms by dividing the number of observations screened by both algorithms by the number of observations screened by one of the algorithms. The larger the value of these fractions the less unique screening information each algorithm is providing. For example, for a given two flags a fraction of 0.5 indicates that half of the observations screened by one flag are also screened by another. These fractions for every algorithm pair are displayed in figure 6.

Figure 6 shows that the majority of fractions are less than 0.5 with many pairs of algorithms having very small fractions indicating complementary screening information. The pairs of RFI flags which screen out the highest number of shared observations (greater than 0.5) are combinations of flags 3, 7, 8 and 10. These are the intensity T3, spatial variability, high pass filter and intensity T4 algorithms. Some level of correlation between the different algorithms is inevitable given that the strongest RFI sources will be detected by multiple algorithms. However, the generally low values for the majority of pairs of algorithms in figure 6, particularly for flags 2, 6 and 11 indicate the complementarity of the algorithms and the power of the GRDS approach of applying multiple different algorithms to the same data.

3.2. Gridded maps

Gridded maps of first-guess departure statistics are formed by splitting the globe up into grid boxes of a fixed size. For the global maps in this report the grid boxes are 1 degree by 1 degree and for the regional maps (see section 3.4) they are 0.5 degree by 0.5 degree. For each grid box all of the observations whose locations are within that grid box are considered as a sample. Then the first-guess departure statistics are calculated based on this sample. Using a month of data means that each grid box has between 700 and 900 observations in its sample leading to reliable and robust statistics for each grid box.

The top left panels of figures 7 and 8 show that with no RFI screening there are large areas of increased standard deviations of first-guess departures over South-Eastern Europe, East Africa, the Middle East, India and South Korea. These hot spots on the maps are one of the clearest visualisations of the effects of RFI on the SMOS data and they correlate with the geographical distribution of known RFI sources. Therefore, the reduction in size and magnitude of these hot spots is a good indicator of the performance of the various RFI screening methods. The top right panels of figures 7 and 8 show that the current screening certainly reduces the magnitude of the hot spots, indicating it is able to screen out some of the worst RFI-affected SMOS observations. However, there are still increased standard deviations of first-guess departures in these areas with the current screening, especially when compared to areas with many fewer or no RFI sources such are the Americas and Australia.

The lower three panels of figures 7 and 8 show that the GRDS screening reduces the magnitude and area of the hot spots more dramatically than the current screening with the best results appearing to come from the most aggressive threshold 1. Even this screening is not perfect, for example there are still some remaining areas of increased first-guess departures over South-Eastern Europe for H polarisation (see section 3.4.1 for more details). However, for V polarisation, the first-guess departure values are similar all over the globe with the threshold 1 screening, indicating that the majority of RFI-affected observations are being screened out, bringing the data quality in these areas in to line with the

data quality in areas unaffected by RFI. These results are some of the most striking and the strongest indication that the GRDS is doing a very good job at screening out almost all of the RFI-affected observations which can be detected when the observations are compared to the NWP model equivalent values.
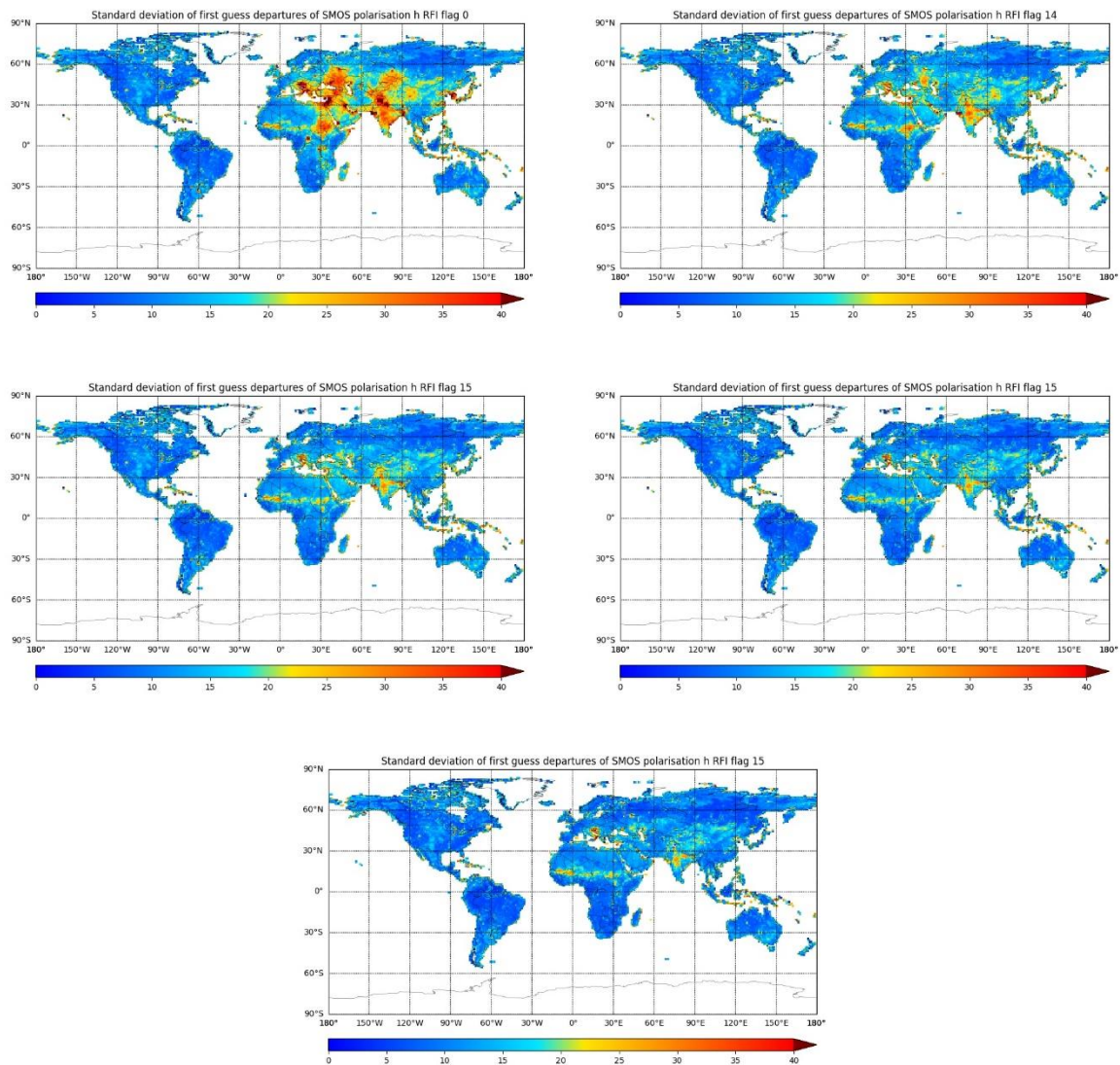

Figure 7: Gridded maps of standard deviation of SMOS first-guess departures at H polarisation (see main text for a full explanation for how these maps are produced) with different RFI screening applied. Upper left: no RFI screening; upper right: current RFI screening; middle left: GRDS threshold 3 screening; middle right: GRDS threshold 2 screening; bottom: GRDS threshold 1 screening. The sample of data for all plots is the same and comes from between 1st July 2019 and 31st July 2019
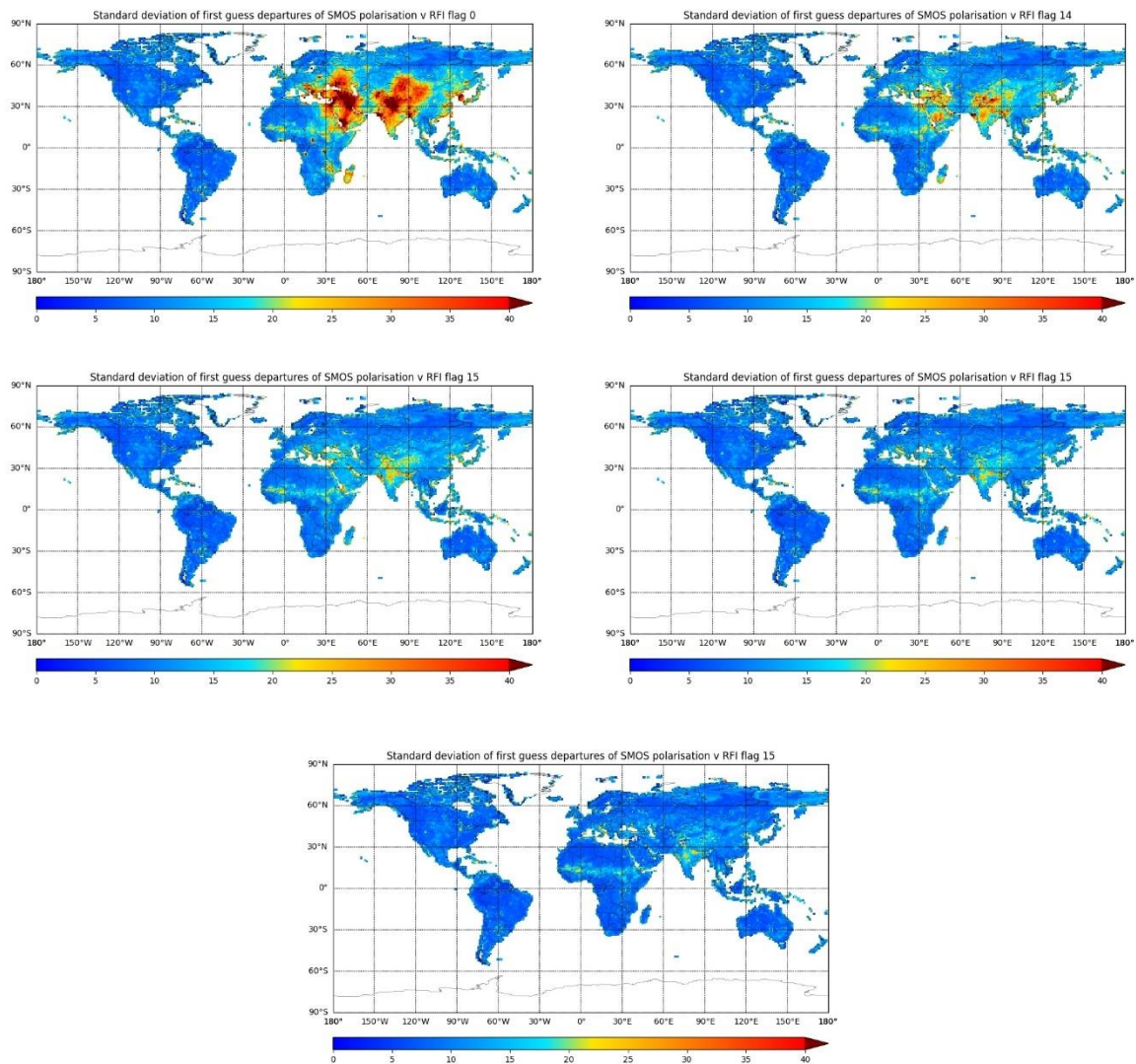
Figure 8: As figure 7 but for V polarisation

3.3. Histograms

Figure 9 shows the effect of the different levels of screening on the SMOS first-guess departure distribution. It shows that the current screening does reduce both of the tails of the distribution slightly, but significantly large tails still remain. The three levels of GRDS screening further reduce the tails with more significant effects as the thresholds are made more aggressive. Observations in the tails of the first-guess departure distribution are those which are in gross disagreement with the model. The most likely reason this gross disagreement is RFI present in the observations which isn't present in the model, therefore a reduction of observations in the tails indicates that RFI-affected observations are being screened out. Notably, the GRDS screening also make the histograms more symmetric and the distributions become more Gaussian. This also indicates RFI-affected observations, which are likely to skew the distribution, are being successfully screened out.

One slight concern with the most aggressive threshold 1 screening is that in the zoomed histogram it is clear that the peak of the distribution is being significantly reduced (noting the logarithmic y axis). Observations near the peak of the distribution are generally in good agreement with the model and therefore are less likely to be affected by RFI. Therefore, this may indicate that there are false alarms when using the most aggressive threshold 1 screening. On the other hand, there may be low levels of RFI that are not affecting the SMOS first-guess departures too much but are only being (correctly) screened out by the most aggressive threshold 1. Further investigations into false alarms can be found in section 3.4.2.
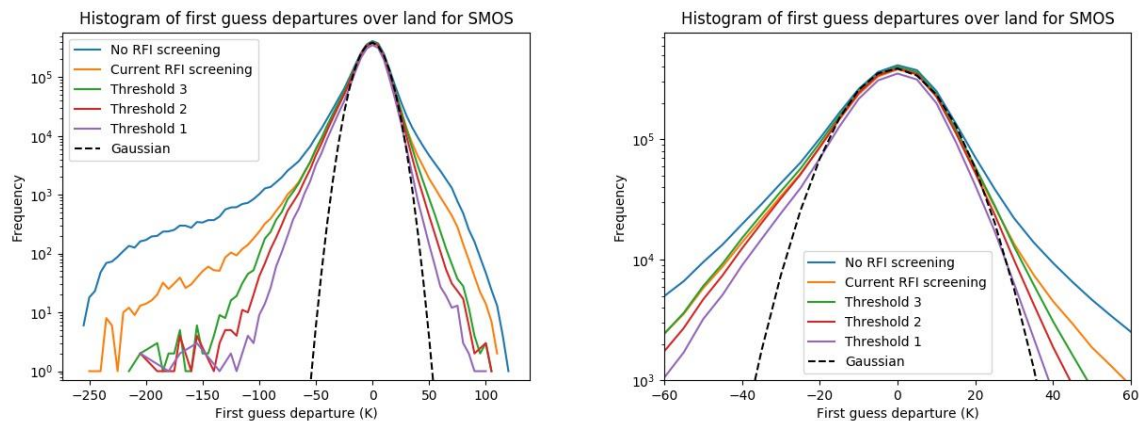

Figure 9: Histograms of SMOS first-guess departures over land at V polarisation and incidence angles of 40°±0.5°. The different levels of screening are: no screening (blue); current screening (orange); GRDS threshold 3 screening (green); GRDS threshold 2 screening (red); and GRDS threshold 1 screening (purple). The black dashed line shows the Gaussian pdf which best fits the peak of the SMOS distributions. The right panel shows a zoomed version of the left panel. The data is from 1st July to 31st July 2019, note the logarithmic y axis

The Gaussian pdf plotted in figure 9 which provides the best match of the SMOS distribution near the peak has a standard deviation of 10.5K. This provides an estimate of the true SMOS first-guess departure standard deviation (for this polarisation and incidence angle) without the effects of RFI and is in line with the standard deviation of first-guess departures over areas non affected by RFI (e.g. 10.37K over Australia, see figure 12). Table 1 shows that the global standard deviation for V polarisation and incidence angle of 40° is 13.7K which is significantly larger than the estimate of 10.5K for non-RFI contaminated observations. This indicates there may still be undetected RFI affecting the filtered observations, although there will also be contributions from errors in the land surface modelling, CMEM and representation errors that could be contributing to this mismatch. The fact that the histograms are much more symmetric with the GRDS screening suggests that the vast majority of RFI-affected observations are being successfully screened out.

3.4. Regional analyses

3.4.1. South-Eastern Europe

As shown in figures 7 and 8, particularly the top panels, South-Eastern Europe is an area which has a significant number of strong RFI sources at L-band. The increased standard deviation of first-guess

departures over this area indicates this and the current screening is unable to completely remove the signature of the RFI on the data. Therefore, it makes a good case study to perform a more localised analysis of how the GRDS is performing.
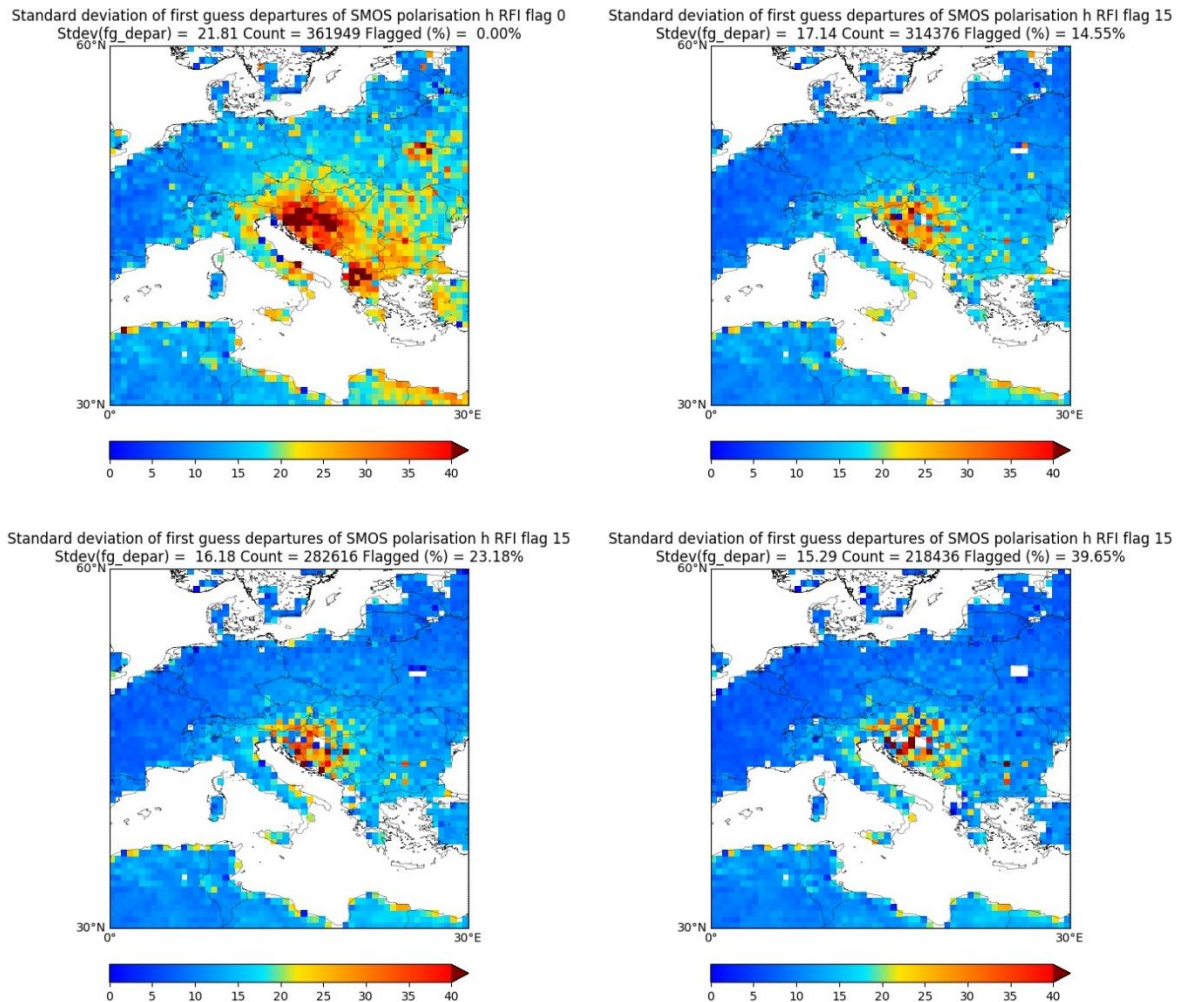

Figure 10: Gridded maps of standard deviation of SMOS first-guess departures at H polarisation over South-Eastern Europe with different RFI screening applied. The titles of the plots contain summary statistics for the whole area. Upper left: no RFI screening; upper right: GRDS threshold 3 screening; lower left: GRDS threshold 2 screening; lower right: GRDS threshold 1 screening. The sample of data for all plots is the same and comes from between 1st July 2019 and 31st July 2019

The top left panel of figure 10 shows the effect that RFI has in this region at H polarisation with large areas of standard deviations of first-guess departure exceeding 40K, particularly over Croatia and Albania, but with effects spreading across the whole of Eastern Europe. There is also another source in the North-West of Ukraine. The area-wide standard deviation of first-guess departures is 21.81K which is significantly larger than the values seen in non-RFI-affected areas. The other three panels of figure 10 show that the GRDS screening is screening out much of the worst affected data and having a significant effect on the first-guess departures. Threshold 1 does the best job screening out almost 40% of the data whilst reducing the standard deviation of first-guess departures to 15.29K. Clearly there are

still some contaminated observations and 15.29K is still larger than the values seen in non-RFI-affected areas (~13.92K over Australia, not shown), but the remaining data is a lot more usable than with no screening. Notably threshold 1 is able to completely screen out the data over the apparent RFI source in North-West Ukraine. Another key aspect here is that the remaining observations in areas away from the RFI sources have significantly better first-guess departure statistics which are more in line with those in non-RFI-affected areas.
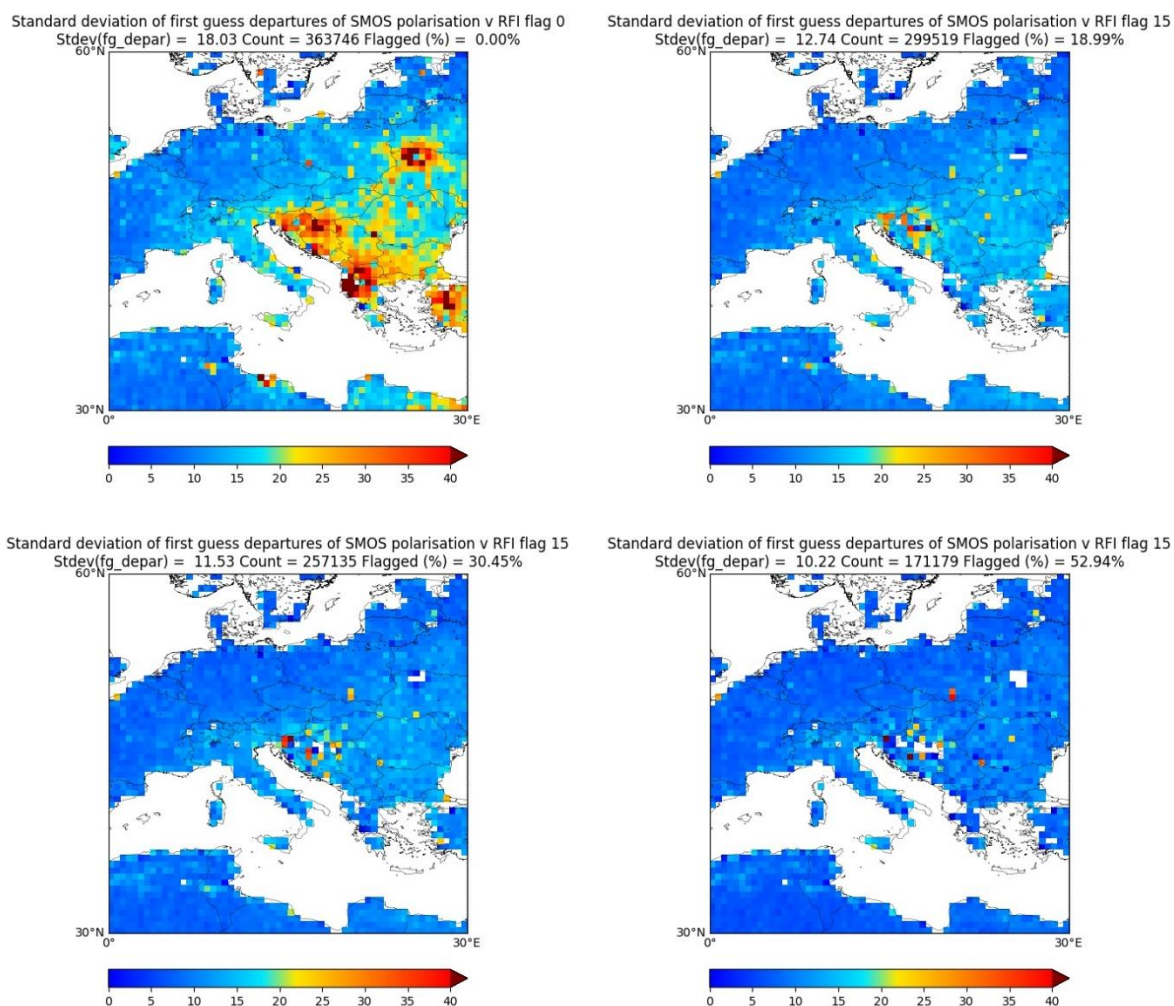

Figure 11: As figure 10 but for V polarisation

Figure 11 shows that for V polarisation the RFI in this area is slightly less intense with fewer pixels exceeding standard deviations of first-guess departure of 40K and an area-wide average of 18.03K. In this case the GRDS almost completely removes the signature of the RFI albeit, with threshold 1, by screening out more than half of the data (52.94%) in the region. It could be argued that screening out so much data is justified here, as the area-wide standard deviation of first-guess departures is reduced to 10.22K which is comparable to the corresponding values in non-RFI-affected areas (e.g. 10.37K over Australia, see figure 12).

This regional analysis shows that the GRDS appears to work slightly better for SMOS observations with V polarisation than H polarisation. As well as removing RFI-affected observations over the

sources, the GRDS does a good job of removing observations in the surrounding areas which are still affected by sources in neighbouring areas. For V polarisation the data quality of the screened observations becomes similar to the data quality in areas of the world which aren't affected by RFI.

3.4.2. *Australia*

Australia is an area of the world where no RFI sources at L-band are expected to be present. Therefore, assessing the performance of the GRDS over Australia is an effective way of measuring the false alarm rate, i.e. what percentage of observations are screened for RFI when it is believed no RFI is present. Note that only ascending passes of the satellite are considered here as there is some evidence of RFI affecting descending passes of the satellite in this area.
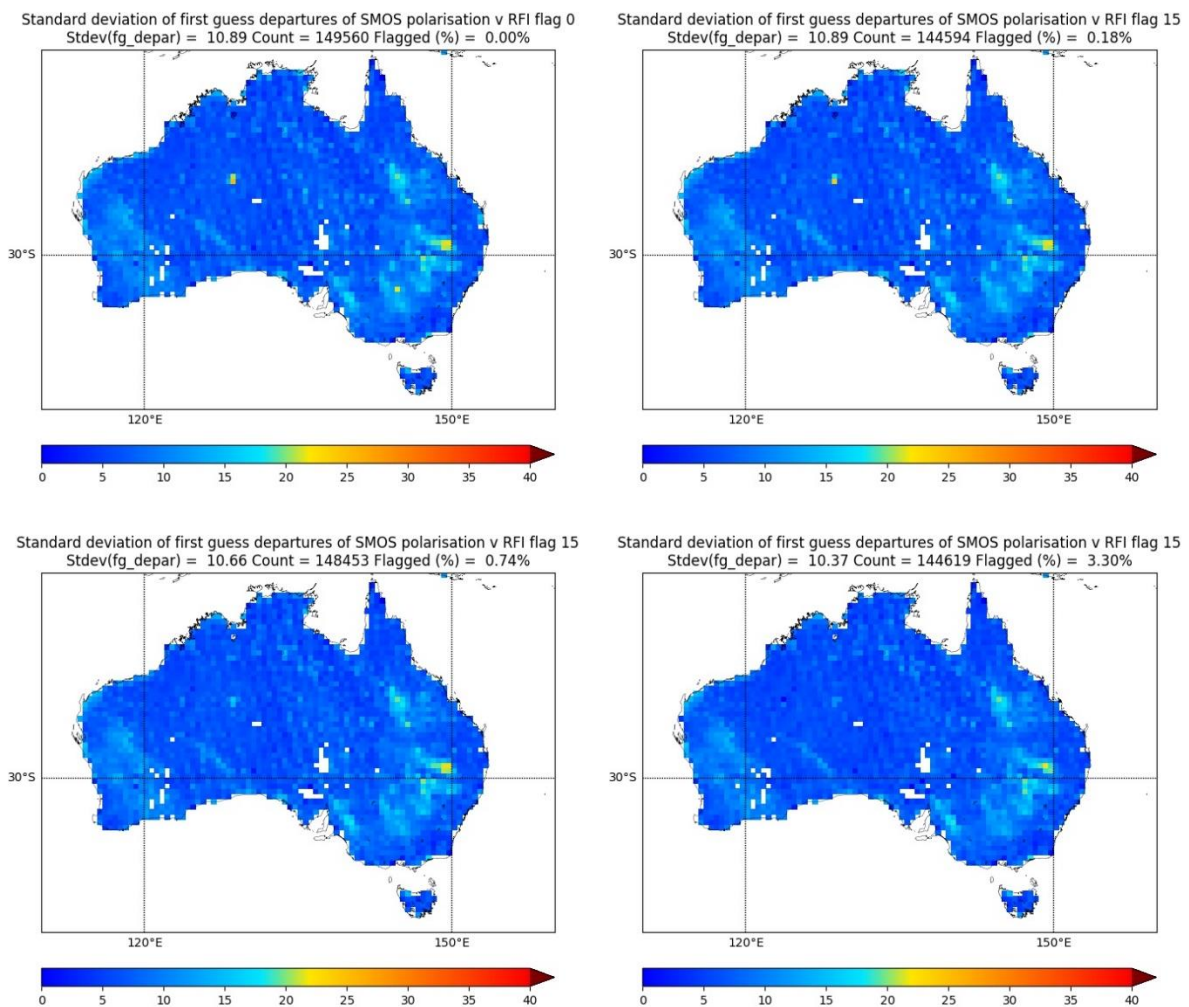

Figure 12: As figure 10 but for Australia and V polarisation

Figure 12 shows that very few V polarisation observations are screened out by the GRDS over Australia. In fact, even with the most aggressive threshold 1, only 3.3% of observations are screened out (results for H polarisation are very similar with 3.88% of observations screened out by GRDS threshold 1, not shown). The effect on the coverage is almost not noticeable and the effect on the standard deviation of first-guess departures is small too with the area-wide value dropping from 10.89K with all observations

to 10.37K when applying the GRDS threshold 1 screening. For thresholds 2 and 3 the effects are even smaller. Although any false alarms are not ideal, this relatively small percentage of false alarms represents a good outcome especially when combined with how effective the GRDS is at removing RFI-affected observations as shown in section 3.4.1.

4. Conclusions

This report has shown that the ground RFI detection system (GRDS) significantly improves the screening of RFI-affected SMOS observations when assessed using the ECMWF IFS NWP model as a reference compared to applying no screening and the current operational RFI screening. The global first-guess departure statistics are most improved when using the most aggressive thresholds within the GRDS and analysis over areas believed to be free from RFI indicate that the false alarm rate is relatively low.

Maps of gridded first-guess departure statistics show that the majority of contaminated data over areas known to be worst affected by RFI such as South-Eastern Europe and the Middle East is successfully screened out. Moreover, the first-guess departure statistics of the data which passes the screening in these areas is then of comparable quality to the data in areas thought to be completely free of RFI at L-band such as the Americas and Australia.

Analysis of the effects of the individual algorithms which make up the GRDS indicate that no single algorithm dominates and that the different algorithms bring complementary screening information. This justifies and validates the design choice of the GRDS which applies multiple different algorithms to the same data.

Overall, the concept of the GRDS has been proven when applied to SMOS observations. The use of this kind of system will be invaluable when attempting to directly assimilate SMOS brightness temperature observations in RFI-affected areas as it will avoid RFI-affected data contaminating the NWP analysis and forecasts.

Appendix A - Summary of results from intermediate versions of GRDS

In this appendix a summary of the results from previous versions of the GRDS are presented with the aim to illustrate the significant improvements made to the GRDS as a direct consequence of data analysis performed within an NWP system.

The data samples produced using the previous versions of the GRDS were smaller than the final month-long sample to speed up the acquisition, processing and experiment run times. These samples covered a 36 hour period between 00UTC on 15th June 2019 and 12UTC on 16th June 2019. The data samples contained RFI flagging information in a similar way to the final data sample as described in section 2.2. The RFI flagging information came from 9 new GRDS algorithms (with slightly different definitions from those in table 1) and with three different thresholds (with different threshold values but a similar

definition to those described in table 2). To simplify the comparisons between different versions most of the results shown here will focus on the intermediate threshold 2. In total, 4 different samples (including the final dataset) from different versions of the GRDS were provided. Here, just the first three are compared because the final data sample comes from a different period which doesn't coincide with the 36 hour period for the first three versions.
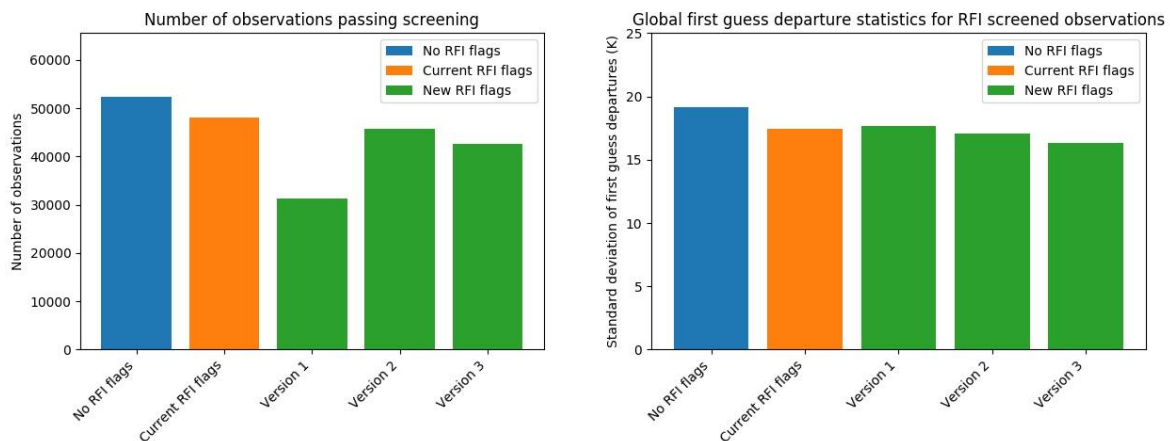

Figure 13: Bar charts showing the number of observations passing RFI screening (left panel) and the global standard deviation of first-guess departures (right panel) for different versions of RFI screening: No screening (blue bar); current screening (orange bar); different versions of GRDS screening (green bars). The data is accumulated from 00UTC on 15th June 2019 to 12UTC on 16th June 2019
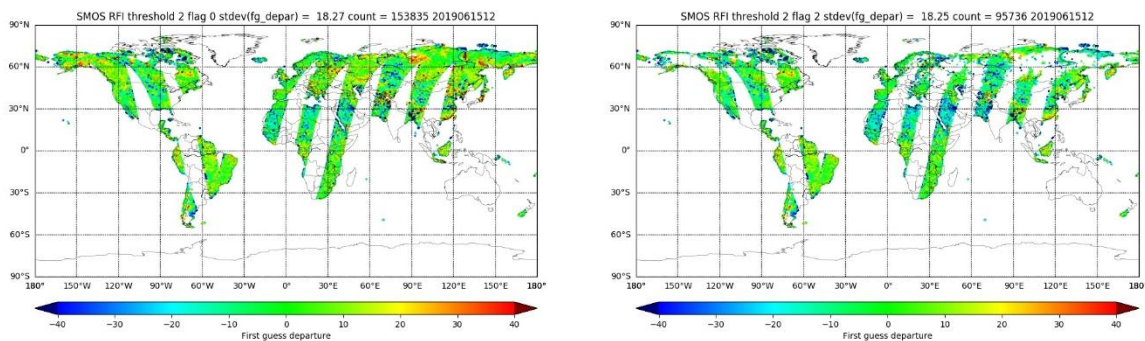

Figure 14: Maps of SMOS first-guess departures with no RFI screening (left panel) and with GRDS version 1 RFI flag 2 screening (right panel). Note the large areas of screened out data over high latitude areas such as Siberia and Canada. Data is accumulated between 09UTC 15th June 2019 and 21UTC 15th June 2019.

Figure 13 shows that in version 1 of the GRDS screening almost half of all observations were screened out, many more observations than with the current RFI flags. The effect of this screening did reduce the standard deviation of first-guess departures but not by as much as the current screening. Figure 14 shows this was due to one particular algorithm, RFI flag 2, screening many observations at high latitudes where RFI sources are not expected to be present. This indicated there were many false alarms in the GRDS version 1 and led to significant improvements in version 2 where figure 13 shows only slightly more screened observations than the current flags and a slightly larger reduction in the standard deviation of

first-guess departures. Version 3 was an additional improvement on version 2 with slightly more observations screened but a further significant reduction in the standard deviation of first-guess departures.

As introduced in section 3.1 the effectiveness of each algorithm can be measured by dividing the reduction in standard deviation of first-guess departures by the number of observations screened out to calculate a so-called effectiveness metric. The exact values of this metric are meaningless but when compared between different algorithms it can indicate which algorithms are more or less effective. Figure 15 shows the effectiveness metric for the different algorithms and different GRDS versions. It shows that in the first GRDS version only 4 of the 9 algorithms showed any kind of effectiveness. This was improved in version 2 with 7 of the algorithms being effective. However, it was clear that RFI flag 10 was dominant in this version, with RFI flag 2 also significantly more effective than the other algorithms. In version 3 (and the final version, as shown in figure 6) the effectiveness of each of the algorithms are more balanced which led to more complementarity between the different algorithms and a more effective overall system.
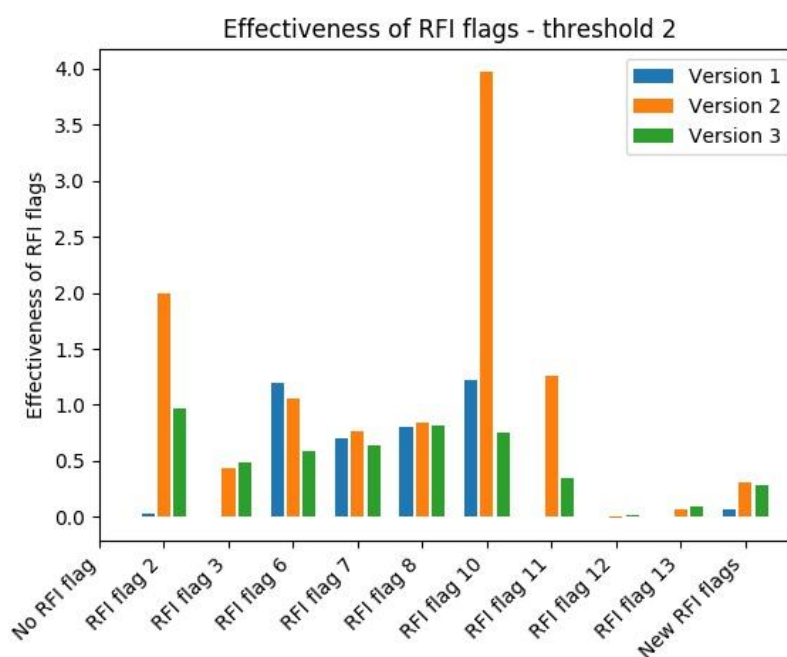

Figure 15: Bar chart showing the effectiveness metric (see main text for definition) for SMOS observations at H polarisation and incidence angles of 40°±0.5° for different GRDS algorithms and versions. The set of bars farthest to the right represents the combination of all of the GRDS (new) flags. The data is accumulated from 00UTC 15th June 2019 to 12UTC 16th June 2019

References

de Rosnay, P., M. Dragosavac, M. Drusch, A. Gutiérrez, M. Rodríguez López, N. Wright, J. Muñoz Sabater, Raffaele Crapolicchio: SMOS NRT BUFR specification, 2015. https://earth.esa.int/documents/10174/1854583/SMOS_NRT_BUFR_Specification

Muñoz Sabater J., M. Dahoui, P. de Rosnay, L. Isaksen: Technical Note, Phase II, WP1100: "*SMOS Monitoring Report number III: Dec-2011 - Dec-2012"*. ECMWF ESA/ESRIN Contract 4000101703/10/NL/FF/fk, April 2013

Oliva, R. Technical Note on the RFI detection algorithm development. ESA contract report 4000127267/19/NL/AF, May 2020.

Weston, P., P. de Rosnay, S. English. GRDS Test-bed plan. ESA contract report 4000127267/19/NL/AF, November 2020.